On the representaion of reinforced concrete structures in FDTD-based simulations to compute lightning-induced magnetic fields

Susana Naranjo-Villamil, Christophe Guiffaut, Julien Gazave, Eric Piedallu, Alain Reineix, Boris Marquois

Accepted Manuscript
On the representation of reinforced concrete structures in FDTD-based simulations to compute lightning-induced magnetic fields.
Susana Naranjo-Villamil, Christophe Guiffaut, Julien Gazave, Eric Piedallu, Alain Reineix, Boris Marquois,
DOI: 10.1016/j.epsr.2024.
Reference:
Publisher: ELSEVIER
To appear in: Electric Power Systems Research
Accepted date: May 2024
Date of Publication: May 2024 (Volume 230)
Reference:
Please cite this article as: Susana Naranjo-Villamil, Christophe Guiffaut, Julien Gazave, Eric Piedallu, Alain Reineix, Boris Marquois,
On the representation of reinforced concrete structures in FDTD-based simulations to compute lightning-induced magnetic fields, Electric Power Systems Research, Volume 230, 2024, ISSN 0378-7796,
https://doi.org/10.1016/j.epsr.2024.110235.
Document Version: Early version, also known as pre-print

On the Representation of Reinforced Concrete Structures in FDTD-Based Simulations to Compute Lightning-Induced Magnetic Fields

Susana Naranjo Villamil[a,*], Christophe Guiffaut[b], Julien Gazave[a], Eric Piedallu[a], Alain Reineix[b], Boris Marquois[c]

[a] *EDF Power Networks Lab, EDF Group, Av. des Renardières, Moret-Loing-et-Orvanne, 77250, Ile-de-France, France*
[b] *CEM et Diffraction, XLIM Research Institute, 123 Av. Albert Thomas, Limoges, 87000, Haute-Vienne, France*
[c] *EDF / DIPNN / DI / TEGG, EDF Group, 905 Av. du Camp de Menthe, Aix-en-Provence, 13090, Provence-Alpes-Côte d'Azur, France*

Abstract

Reinforced concrete structures are generally well protected against the adverse effects of a direct lightning strike. Nevertheless, when it occurs, the electromagnetic field generated by the lighting current flowing through their reinforcement can cause a malfunction of sensitive electronic devices. The electromagnetic field can be estimated using full-wave methods, although the accuracy of the estimation depends on the representatives of the model, which is why experimental validation is essential. This paper presents the numerical model of a reinforced concrete structure where a current was injected to emulate a direct lightning strike. Full-wave simulations are conducted using TEMSI-FD and the results are compared to the measurements made at the testing facility of EDF TEGG. The simulation results were in good agreement with the measurements, especially when the soil was used as the return path for the current.

Keywords: lightning, magnetic field, reinforced concrete, measurements, finite-difference time-domain method

*Corresponding author
Email address: susana.naranjo-villamil@edf.fr (Susana Naranjo Villamil)

1. Introduction

A direct lightning strike can have diverse mechanical and electrical effects, which is why structures are generally equipped with at least an external lightning protection system. The reinforcement of a building can be considered as part of its protection system since the vertical rebars can work as down-conductors, transporting the lightning current into the ground. However, the current flowing through the reinforcement generates a transient electromagnetic field that may lead to an upset of sensitive electronic devices. In industrial facilities, any temporary malfunction can quickly escalate into an important issue.

Different approaches have been used to estimate the electromagnetic fields generated by a direct lightning strike inside a reinforced concrete building (see e.g., [1, 2, 3, 4, 5, 6]). If the components of the electromagnetic environment are modeled appropriately, the most accurate results are generally obtained using full-wave methods, such as the finite-difference time-domain (FDTD) method and the method of moments (MoM). These two methods have gained popularity in the lightning community due to their capabilities to handle three-dimensional structures, cables, and wiring structures. When modeling complex environments, the FDTD method is particularly advantageous because the computation time depends on the discretization of the domain and not on the number of elements.

Nevertheless, no matter how precisely we try to represent reinforced concrete structures in full-wave simulations, there will always be some uncertainty. For example, the rebars forming the reinforcement have, in theory, a circular cross-section. However, in reality, because of the ribs and the markings, the rebars are not cylindrical. This is most likely negligible for lightning-related studies; yet, the uncertainty of numerous insignificant variables could propagate and result in considerable errors.

Aiming to validate the representation of reinforced concrete buildings in our simulations, we conducted experiments at the testing facility of EDF TEGG. A good agreement between computations and measurements of the magnetic field has already been observed in [7, 8, 9, 10]. The preliminary results of the experiments at the testing facility can be found in [11]. When the paper was written, the magnetic field probe had not been calibrated and the simulations had been conducted using two different solvers in CST Studio Suite [12]: a solver based on the finite integration technique (FIT) [13] and a solver based on the transmission line matrix method (TLM) [14]. In

the simulations, the concrete was not modeled, most of the interconnections between the layers of the reinforcement were not considered, and the rebars were represented as perfectly conducting wires. Also, we had adjusted the current source based on a simple representation of the load. In this paper, we study the distribution of the magnetic field, considering a more elaborated model of the structure at the testing facility. The simulations are carried out using TEMSI-FD [15], a solver based on the FDTD method, and the results are compared to the measurements taking into account transfer function of the magnetic field probe.

2. Testing Facility of EDF TEGG

Figure 1: Reinforced concrete structure at the testing facility of EDF TEGG.

At the testing facility of EDF TEGG, located in the south of France, a reinforced concrete structure was built in 2016 to test the properties of commonly used construction materials. As shown in Figure 1, the structure consists of two adjacent walls perpendicular to each other over a 3.4 m $\times$ 3.4 m slab. The walls are 5 m in height and have a thickness of 50 cm. Note that we have named the walls W1 and W2. The slab has a thickness of 40

Figure 2: Reinforcement of an isolated footing of the structure.

cm and is supported by four symmetrical columns of 50 cm × 50 cm. Each column is connected to an isolated footing of 1.5 m × 1.5 m (see Figure 2). The footings are all connected to a raft foundation of 4.4 m × 4.4 m.

The walls and the slab have a double-layered reinforcing grid with meshes of approximately 25 cm × 20 cm and 25 cm × 25 cm, respectively. As shown in Figure 3, even though the layers are interconnected, the hoops are not always periodically distributed. A more detailed view of the configuration of the reinforcement is shown in Figure 4. The reinforcing grid of the footings and the raft foundation also has meshes of approximately 25 cm × 25 cm. Based on the impedance of the structure (see Figure 5), we can assume that there is good contact between the rebars. Significant differences in the resistance of reinforced concrete structures can be observed, even when the rebars are wire-tied [16]. The impedance of the structure was measured using a Bode 100 vector network analyzer (VNA).

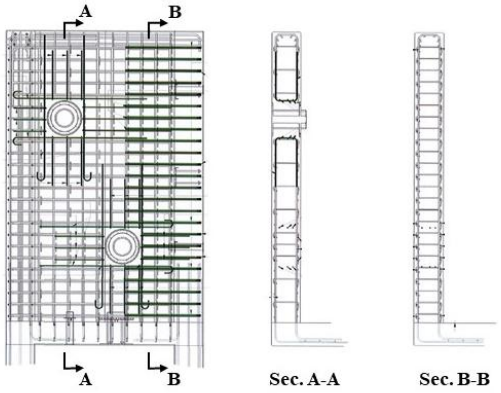

Figure 3: Interconnections between the layers of the reinforcing grid in wall W2.

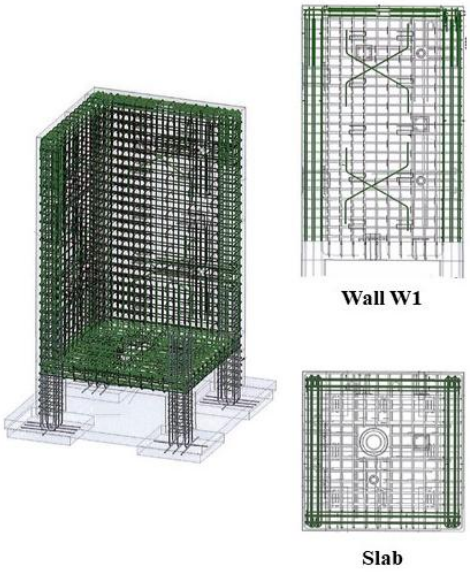

Figure 4: Configuration of the reinforcement of the structure.

The radius of the rebars forming the reinforcing grids varies between 4 mm and 10 mm. In the walls and the outer layer of the slab, we mostly find rebars with a radius of 8 mm, whereas the rebars in the inner layer of the slab have a radius of 10 mm.

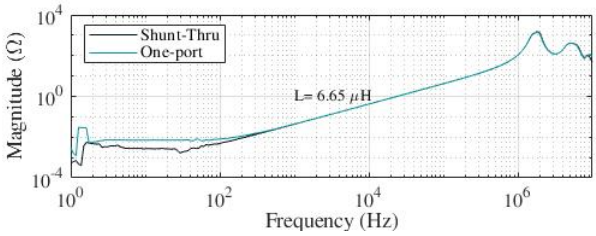

Figure 5: Impedance of the structure measured using a VNA.

At 16 m from the structure, a grounding point for the equipment was created by burying a meshed copper network of 1 m × 1 m at a depth of 1 m (see Figure 6). Using the three-pole method to measure the ground resistance of the grounding point, we obtained values between 8.5 Ω and 12.15 Ω, depending on the distance between the electrodes. Similarly, since

the soil at the facility is not homogeneous, using the Schlumberger method to measure the resistivity of the soil, we obtained values between 47 Ω·m and 56 Ω·m.

Figure 6: Grounding point created for the equipment.

3. Experimental Setup

A 25-meter-long copper braid was connected at the top center of wall W1 to emulate a direct lightning strike to the structure (see Figure 7). The angle between the wall and the braid is approximately 73°. At the other end, the braid was connected to an EMC Partner IMU3000 test system. The current generated by the test system and injected into the reinforcement was measured using a Pearson 110A current monitor.

The IMU3000 test system generates surge impulses as defined in the IEC 61000-4-5 standard [17]. The waveform of the open-circuit voltage has a front time of 1.2 μs and a time to half-value of 50 μs. The waveform of the short-circuit current has a front time of 8 μs and a time to half value of 20 μs. The peak voltage at the output was set to 4 kV.

Two different configurations were considered for the return path:

- Case A: A low-resistance return path was created by means of three 25-meter-long copper braids. As shown in Figure 8, the braids were connected at the bottom of wall W1. In this case, a 10 Ω resistance was added at the output of the generator to reduce the front time of the current injected into the reinforcement.

- Case B: The IMU3000 test system was connected to the grounding point described in the previous section to use the soil as the return path.

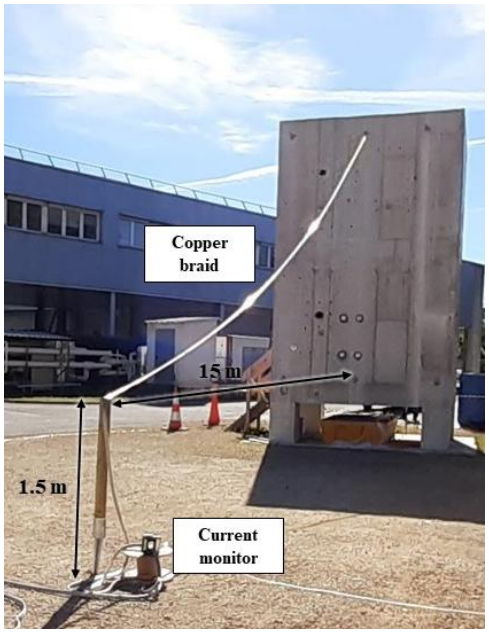

Figure 7: Copper braid used to inject a current into the reinforcement of the structure.

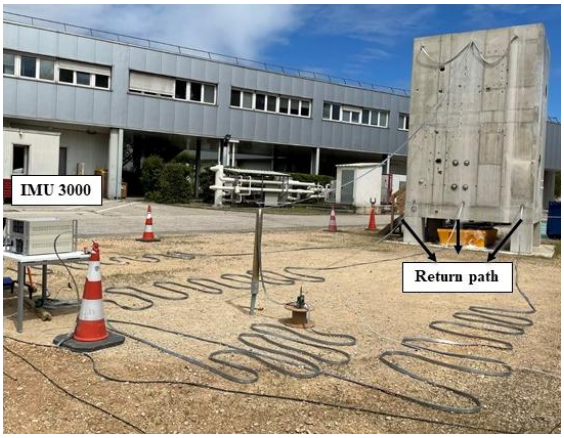

Figure 8: Experimental setup in case A.

As shown in Figure 9, the magnetic field generated by the current flowing through the reinforcement was measured at 18 observation points behind wall W1 using a unidirectional magnetic field probe. Half of the points were 15 cm away from the wall, and the other half, 60 cm away from the wall. The 9 points at each distance are designated by letters A to I (see Figure 10).

The magnetic field probe was connected to an optical Messtechnik U1/14-30M-Iv transmitter that amplified the signal by 24 dB and transmitted it to a Yokogawa DL9240 oscilloscope.

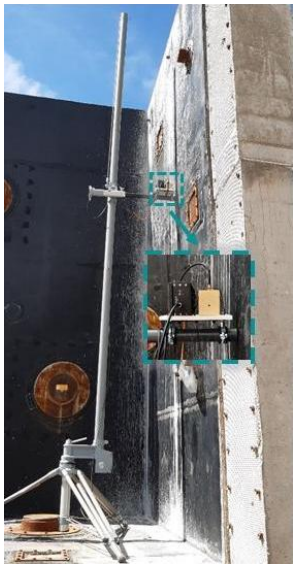

Figure 9: Measurement of the magnetic fields behind wall W1.

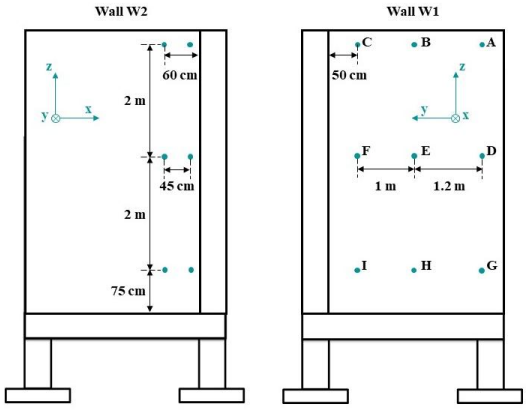

Figure 10: Points at which the magnetic field was measured.

3.1. Magnetic Field Probe

To the best of the authors' knowledge, the magnetic field probe had a sensitivity of approximately 4 mV/(A·m^{-1}). To verify, we estimated the transfer function of the probe using the stripline at the XLIM Research Institute and a VNA. The setup is shown in Figure 11. As shown in Figure 12, the probe behaves as a high-pass filter, attenuating the low-frequency content of the magnetic field. The latter implies that some information was lost and we cannot entirely reconstruct the signals that we had measured. Hence, we will have to focus on the peak-values of the magnetic field to compare the results of the simulations and the measurements.

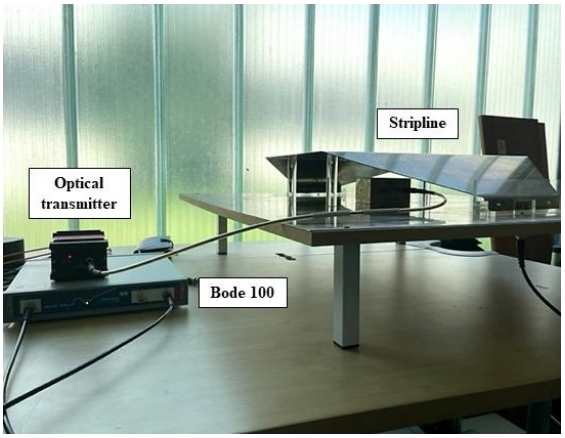

Figure 11: Experimental setup for the estimation of the transfer function of the magnetic field probe.

4. Numerical Model

The numerical model of the experimental setup at the testing facility is shown in Figure 13. The volume of the analysis space is set to 25.5 m × 8 m × 9.8 m, and to assume an open space, all the external surfaces are defined as perfectly matched layers (PML)[18]. The volume is divided into uniform cells of 10 cm × 10 cm × 10 cm.

The soil is modeled as a homogeneous dialectic material with a relative permittivity of 10 and a resistivity of 50 Ω·m. Since the structure was built in the last 10 years, one would expect the concrete to have a moisture content of about 5.5%. Thus, the concrete is modeled as a dielectric material

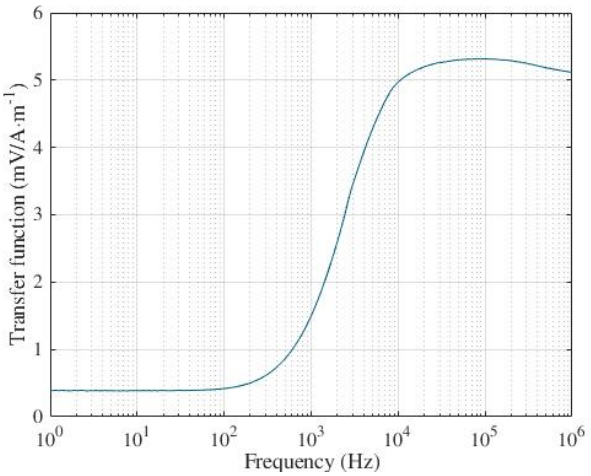

Figure 12: Transfer function of the magnetic field probe.

with a relative permittivity of 8.6 and a conductivity of 0.005 S/m. These values correspond to the static values estimated by Sandrolini *et al.*[19] for an extended Debye model.

All the conductors are modeled as thin-wires [20]. The linear resistance of the wires is calculated as $1/(\pi \times r^2 \times \sigma_m)$, where r is the radius of the wire and σ_m is the material's conductivity. The conductivity of copper and steel is set to 59.6×10^6 S/m and 8.33×10^6 S/m, respectively.

The radius of the wires representing the braids is calculated from their cross-sectional area. The resistance and inductance of a flat braid are lower than those of a round conductor of the same cross-sectional area. Yet, we consider these differences to be negligible and set the radius to 7 mm.

The meshed network of the grounding point is represented by a grid with meshes of 10 cm $\times$ 10 cm. The grid is formed by wires with a radius of 2 mm.

Only the vertical and horizontal rebars are considered to represent the reinforcement of the structure. The double-layered grid of the walls is assumed to be symmetrical and identical. The radius of the wires is set to 8 mm. For the double-layered grid of the slab, we used wires with radii of 8 mm and 10 mm. At the edges of both the walls and the slab, the layers of the reinforcing grids are interconnected at every intersection. The layers are otherwise interconnected at one out of two intersections. The columns and the footings are represented using wires with radii of 5 mm and 10 mm. The

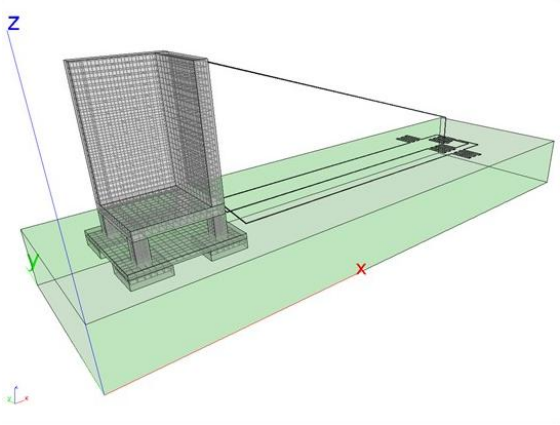

(a)

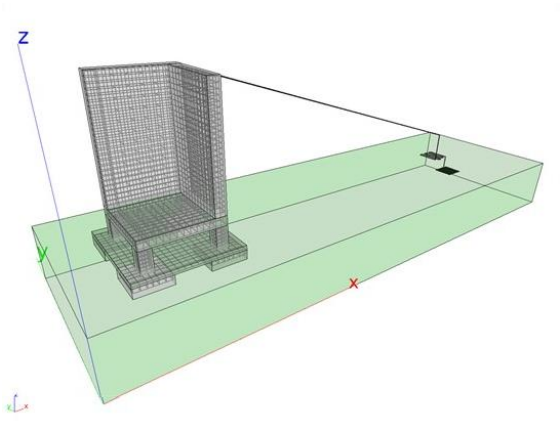

(b)

Figure 13: Numerical model of the experimental setup at the testing facility (a) Case A. (b) Case B.

raft foundation is represented using wires with a radius of 6 mm.

4.1. Voltage Generator

The IMU3000 test system is modeled as the circuit in Figure 14. The pulse voltage source in the circuit starts at time zero and takes 9 μs to rise from 0 V to 4240 V. This circuit reproduces the 1.2/50 μs voltage surge with a peak-value of 4 kV at open-circuit conditions and the 8/20 μs current surge into a short-circuit.

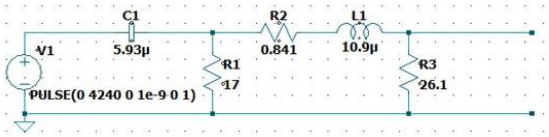

Figure 14: Model of the voltage generator implemented in TEMSI-FD.

Preliminary simulations were carried out in TEMSI-FD before implementing the model of the test system. Instead of the circuit, a voltage surge with a Gaussian waveform was defined to compute the impedance of what would be the load connected to the terminals of the test system. Note that in these simulations, the 10-Ω-resistance added in case A was not modeled.

Figure 15 shows that the simple representation of the load suggested in [11] is not accurate. In case A, the resistance could indeed be neglected and in case B, the resistance computed is of the same order of magnitude. However, the difference between the inductance in case A and case B is 21.66 μH, which proves that there is more to calculating the impedance of the return path than we expected. The coupling between the braids should not be neglected in case A.

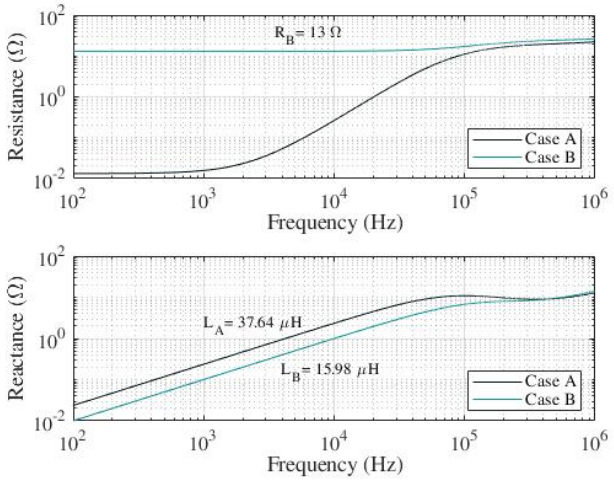

Figure 15: Impedance at the terminals of the generator computed using TEMSI-FD.

Nevertheless, and without modifying the parameters of the circuit, when the model of the test system was implemented, the currents computed using

TEMSI-FD were in good agreement with the currents measured at the testing facility (see Figure 16). At least for the high-frequency part of the response, we could expect to obtain similar values.

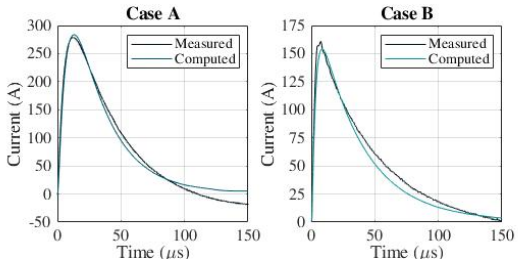

Figure 16: Current injected into the reinforcement of the structure.

5. Results

5.1. Simulations

The magnetic fields computed at the observation points are shown in Figure 17. It is important to note that these fields were computed in the middle of the FDTD cell; thus, they are an approximation of the fields at the positions defined in Figure 10.

It is well-known that when a current flows through the reinforcement of an enclosed structure, the front time of the magnetic field generated inside the structure is significantly longer than the front time of the current. Since the structure at the testing facility only has two walls, the waveforms of the magnetic field and the currents are alike.

It is also interesting to observe that the overall tendencies are similar, although the currents injected into the reinforcement are different in cases A and B. In general, the y-component of the magnetic field is predominant because the current flows downwards. Yet, the z-component of the magnetic field is higher at points C and F, probably because of the partial current flowing towards wall W2 before heading down to the ground.

Figure 18 shows that even in case A, where the braids are connected at the bottom of wall W1, there is a current flowing toward wall W2, and still, an important part of the current is diverted to the outer vertical edges of the walls. Because of the current displacement phenomenon, there is a high magnetic field at points A, D, and G. One would then expect the field to be as high at points F and I; however, Figure 19 shows that the magnetic field

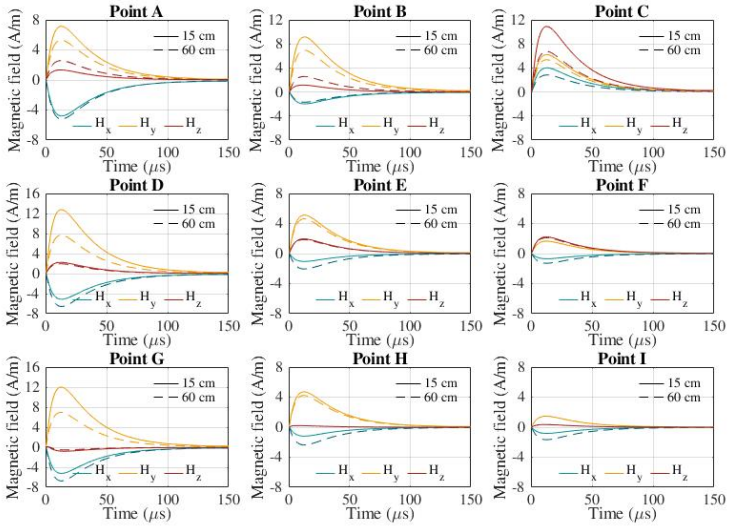

(a)

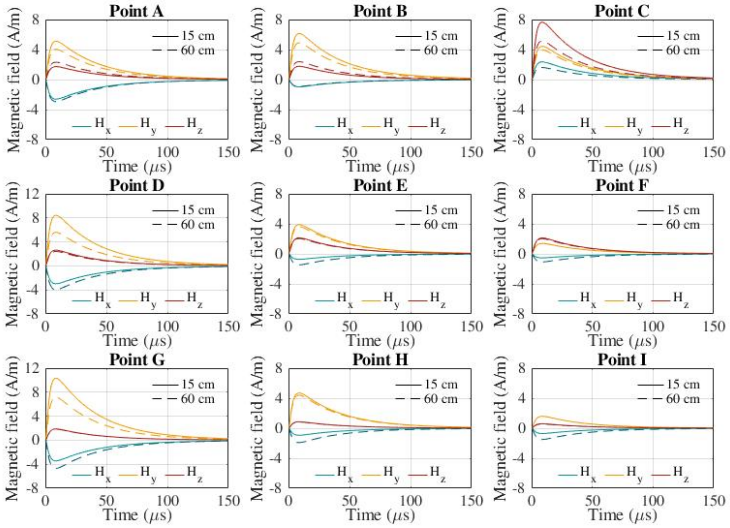

(b)

Figure 17: Magnetic fields computed using TEMSI-FD.(a) Case A. (b) Case B.

strength ($\sqrt{H_x^2 + H_y^2 + H_z^2}$) decreases with the distance to the top of the wall at points which are close to the corner. This is because of the superposition

of the fields generated by the currents flowing through the walls. Notice for example that the field at 60 cm is higher than at 15 cm at points F and I.

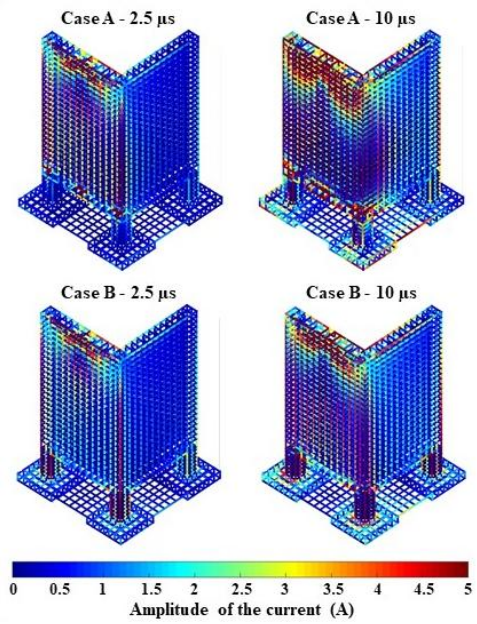

Figure 18: Current distribution in the reinforcement of the structure.

The peak-values in Table 1 highlight the main difference between the fields computed in cases A and B. As expected, the peak-values of the magnetic field in case B are generally lower because the amplitude of the current injected into the reinforcement is also lower. Nevertheless, the proportions are different at the points close to the slab. Close to the slab, the fields in cases A and B are comparable, probably because of a higher current flowing through the slab in case B.

5.2. Measurements

As discussed in section 3.1, the low-frequency part of the signal measured using the probe is not representative of the magnetic field. For example, the zero-crossing one can observe in Figure 20 is not consistent with the phenomenon. Hence, to compare the peak-values of the magnetic fields, we apply the transfer function of the probe to the magnetic fields computed using TEMSI-FD. First, we use the Matrix Pencil method [21] to extrapolate and approximate the response in the frequency domain. Then, we multiply the

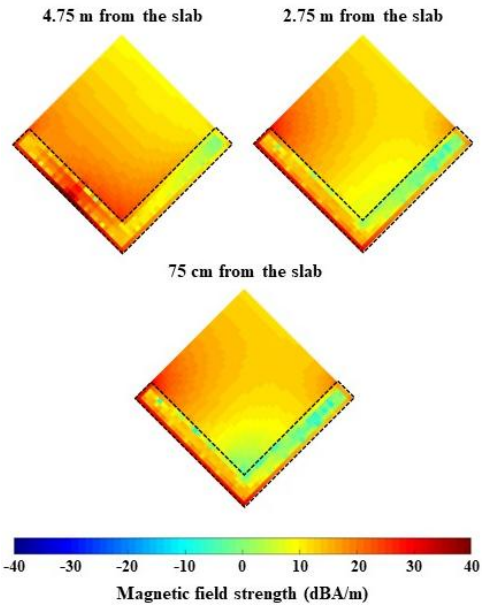

Figure 19: Magnetic field strength at 10 μs in case A.

response by the transfer function of the magnetic field probe. And finally, we perform an inverse Fourier transform and detect the maximum amplitude.

The values obtained for the y-component of the magnetic fields are shown in Figure 21. Note that the amplitude is given in millivolts. Given that the probe is unidirectional, only the y-component of the magnetic fields was measured at all the observation points. If we divide these values by the corresponding peak-values of the computed magnetic fields, we obtain an average of 4.13 mV/(A·m^{-1}). As we had previously assumed, the probe's sensitivity is indeed around 4 mV/(A·m^{-1}) at the frequency of interest.

The values calculated in cases A and B are on average 4.68 mV and 2.09 mV higher than the values measured at the testing facility. We could then suppose that, considering a sensitivity of 4.13 mV/(A·m^{-1}), the fields computed using TEMSI-FD are overestimated by approximately 1.13 A/m and 0.5 A/m in cases A and B, respectively. This already shows a considerable improvement compared to the results presented in [11]. However, since we are comparing small values, the relative error is still non-negligible: 29.6% in case A and 13.7% in case B.

A small part of the error can be attributed to the size of the FDTD cell.

Table 1: Peak-Values of the Magnetic Fields Computed Using TEMSI-FD.

Point	Case A (A/m)			Case B (A/m)		
	H_x	H_y	H_z	H_x	H_y	H_z
A_{15}	-4.79	7.15	1.34	-2.61	5.11	1.73
A_{60}	-5.21	5.30	2.57	-2.93	4.03	2.31
B_{15}	-1.97	9.17	1.16	-0.97	6.14	1.77
B_{60}	-1.70	6.95	2.57	-0.92	4.90	2.38
C_{15}	4.02	6.21	10.90	2.36	4.43	7.64
C_{60}	2.83	5.36	6.75	1.61	3.95	5.15
D_{15}	-5.13	12.77	2.25	-2.97	8.43	2.62
D_{60}	-6.56	7.67	1.96	-3.96	5.59	2.40
E_{15}	-1.05	5.13	1.96	-0.72	3.90	2.14
E_{60}	-2.05	4.64	1.85	-1.46	3.63	2.04
F_{15}	-0.69	1.65	2.22	-0.53	1.39	2.12
F_{60}	-1.28	1.66	2.10	-1.07	1.40	2.03
G_{15}	-5.23	11.99	0.80	-3.44	10.33	1.87
G_{60}	-6.73	6.96	0.53	-4.69	7.14	1.83
H_{15}	-1.19	4.70	0.21	-2.37	4.69	0.86
H_{60}	-2.37	4.23	0.21	-1.91	4.40	0.82
I_{15}	-0.83	1.46	0.36	-1.66	1.59	0.59
I_{60}	-1.66	1.47	0.34	-1.51	1.59	0.55

A smaller cell might increase the accuracy but it will definitely increase the computation time. Finding the right balance is not always straightforward. The higher error in case A is probably due to our representation of the flat braids as thin wires with a circular cross-section. Since the electrical parameters of the soil are know to be frequency-dependant (see e.g. [22]), it is reassuring to find a lower error in case B. We can therefore assume that our representation of reinforced concrete structures in FDTD simulations is appropriate, and keeping in mind that there will always be uncertainty, it

can be used for lightning-related studies.

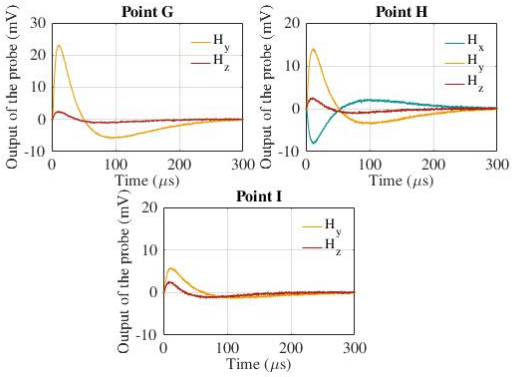

Figure 20: Signals measured using the magnetic field probe at 60 cm in case A.

6. Conclusion

This article presented the numerical model of a reinforced concrete structure at the testing facility of EDF TEGG. A current was injected into the reinforcement of the structure to study the magnetic fields generated by a direct lightning strike. Full-wave simulations were carried out using TEMSI-FD, where all the conductors of the electromagnetic environment were modeled as thin-wires.

The current distribution in the reinforcement of the structure showed that the return path defined for the current influences the results, although other phenomena play an important role. The lowest magnetic fields were observed in the corner formed by the walls because of the superposition of the fields. The highest magnetic fields were observed close to the outer vertical edges of the walls because of the displacement phenomenon. Since the currents flow mainly towards the ground, the y-component of the magnetic fields was the strongest.

There was a good agreement between the simulation results and the measurements made at the testing facility, especially when the soil was used as the return path. As long as the main rebars forming the reinforcing grids are modeled, a good estimation of the magnetic fields can be obtained using TEMSI-FD. The accuracy of the simulations could be improved by reducing the size of the FDTD cell or adapting the characteristics of the wires used to represent the flat braids.

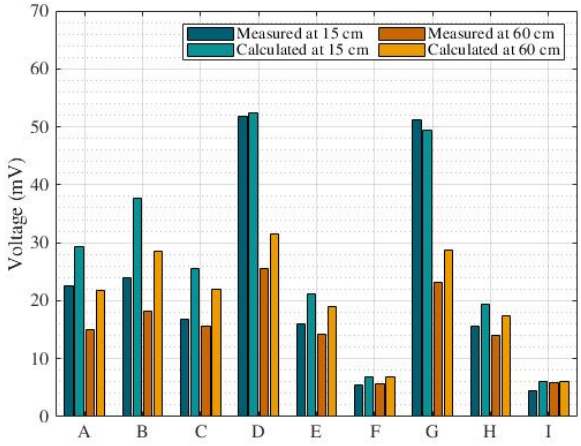

(a)

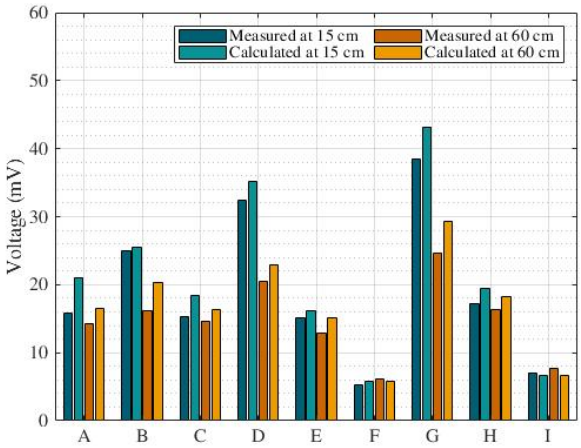

(b)

Figure 21: Peak-values calculated from the simulation results compared to the peak-values measured using the magnetic field probe at the testing facility.(a) Case A. (b) Case B.

References

[1] International Electrotechnical Commission (IEC), IEC 62305-4: Electrical and electronic systems within structures (2010).

[2] A. Orlandi, C. Mazzetti, Z. Flisowski, M. Yarmarkin, Systematic ap-

proach for the analysis of the electromagnetic environment inside a building during lightning strike, IEEE Transactions on Electromagnetic Compatibility 40 (4) (1998) 521–535. doi:10.1109/15.736212.

[3] M. Mardiguian, Lightning-generated fields in reinforced concrete buildings, IEEE EMC Soc. Newsletter 1 (225) (2010) 58–65.

[4] I. Metwally, F. Heidler, Reduction of lightning-induced magnetic fields and voltages inside struck double-layer grid-like shields, IEEE Transactions on Electromagnetic Compatibility 50 (4) (2008) 905–912. doi:10.1109/TEMC.2008.2002575.

[5] A. Tatematsu, F. Rachidi, M. Rubinstein, Analysis of electromagnetic fields inside a reinforced concrete building with layered reinforcing bar due to direct and indirect lightning strikes using the FDTD method, IEEE Transactions on Electromagnetic Compatibility 57 (3) (2015) 405–417. doi:10.1109/TEMC.2015.2400132.

[6] S. Naranjo-Villamil, C. Guiffaut, J. Gazave, A. Reineix, Lightning-induced magnetic fields inside grid-like shields: An improved formula complemented by a polynomial chaos expansion, IEEE Transactions on Electromagnetic Compatibility 63 (2) (2021) 558–570. doi:10.1109/TEMC.2021.3056320.

[7] W. Zischank, F. Heidler, J. Wiesinger, I. Metwally, A. Kern, M. Seevers, Laboratory simulation of direct lightning strokes to a modeled building: measurement of magnetic fields and induced voltages, Journal of Electrostatics 60 (2-4) (2004) 223–232. doi:10.1016/j.elstat.2004.01.011.

[8] I. Metwally, W. Zischank, F. Heidler, Measurement of magnetic fields inside single- and double-layer reinforced concrete buildings during simulated lightning currents, IEEE Transactions on Electromagnetic Compatibility 46 (2) (2004) 208–221. doi:10.1109/TEMC.2004.826894.

[9] A. Kern, F. Heidler, M. Seevers, W. Zischank, Magnetic fields and induced voltages in case of a direct strike—comparison of results obtained from measurements at a scaled building to those of IEC 62305-4, Journal of Electrostatics 65 (5-6) (2007) 379–385. doi:10.1016/j.elstat.2006.09.004.

[10] T. Maksimowicz, K. Aniserowicz, Investigation of models of grid-like shields subjected to lightning electromagnetic field: experiments in the frequency domain, IEEE Transactions on Electromagnetic Compatibility 54 (4) (2012) 826–836. doi:10.1109/TEMC.2011.2174239.

[11] S. Naranjo-Villamil, J. Gazave, E. Piedallu, M. Franchet, B. Marquois, C. Guiffaut, A. Reineix, Measurement of magnetic fields generated by a lightning current flowing through reinforced concrete walls, in: 36th International Conference on Lightning Protection, Cape Town, South Africa, 2022, pp. 291–295.

[12] Dassault Systèmes, CST Studio Suite (2020).

[13] T. Weiland, Finite Integration Method and Discrete Electromagnetism, in: P. Monk, C. Carstensen, S. Funken, W. Hackbusch, R. H. W. Hoppe (Eds.), Computational Electromagnetics, Springer Berlin Heidelberg, Berlin, Heidelberg, 2003, pp. 183–198.

[14] W. Hoefer, The transmission-line matrix method - theory and applications, IEEE Transactions on Microwave Theory and Techniques 33 (10) (1985) 882–893. doi:10.1109/TMTT.1985.1133146.

[15] Institut de recherche XLIM, TEMSI-FD: Time ElectroMagnetic SImulator - Finite Difference (2023).

[16] S. Naranjo-Villamil, E. Piedallu, J. Gazave, C. Guiffaut, A. Reineix, Experimental characterization of reinforced concrete cable ducts, in: 35th International Conference on Lightning Protection and XVI International Symposium on Lightning Protection, Sri Lanka, 2020.

[17] International Electrotechnical Commission (IEC), IEC 61000-4-5: Electromagnetic compatibility (EMC) – Part 4-5: Testing and measurement techniques – Surge immunity test (2014).

[18] J.-P. Berenger, A perfectly matched layer for the absorption of electromagnetic waves, Journal of Computational Physics 114 (2) (1994) 185–200.

[19] L. Sandrolini, U. Reggiani, A. Ogunsola, Modelling the electrical properties of concrete for shielding effectiveness prediction, Journal of

Physics D: Applied Physics 40 (17) (2007) 5366–5372. doi:10.1088/0022-3727/40/17/053.

[20] C. Guiffaut, A. Reineix, B. Pecqueux, New oblique thin wire formalism in the FDTD method with multiwire junctions, IEEE Transactions on Antennas and Propagation 60 (3) (2012) 1458 – 1466. doi:10.1109/TAP.2011.2180304.

[21] T. Sarkar, O. Pereira, Using the matrix pencil method to estimate the parameters of a sum of complex exponentials, IEEE Antennas and Propagation Magazine 37 (1) (1995) 48–55. doi:10.1109/74.370583.

[22] F. H. Silveira, S. Visacro, R. Alipio, A. De Conti, Lightning-Induced Voltages Over Lossy Ground: The Effect of Frequency Dependence of Electrical Parameters of Soil, IEEE Transactions on Electromagnetic Compatibility 56 (5) (2014) 1129–1136. doi:10.1109/TEMC.2014.2313580.